materials

MDPI

Article

Improved Electrochemical Properties of $LiMn_2O_4$-Based Cathode Material Co-Modified by Mg-Doping and Octahedral Morphology

Hongyuan Zhao [1,*], Yongfang Nie [1], Dongyang Que [2], Youzuo Hu [3] and Yongfeng Li [1,*]

[1] School of Mechanical and Electrical Engineering, Henan Institute of Science and Technology, Xinxiang 453003, China
[2] Zhumadian Power Supply Company, State Grid Henan Electric Power Company, Zhumadian 463500, China
[3] Chemistry Department, Lancaster University, Lancaster LA1 4YB, UK
* Correspondence: hongyuanzhao@126.com (H.Z.); lyf16816800@163.com (Y.L.)

Received: 11 August 2019; Accepted: 29 August 2019; Published: 31 August 2019

Abstract: In this work, the spinel $LiMn_2O_4$ cathode material was prepared by high-temperature solid-phase method and further optimized by co-modification strategy based on the Mg-doping and octahedral morphology. The octahedral $LiMn_{1.95}Mg_{0.05}O_4$ sample belongs to the spinel cubic structure with the space group of Fd3m, and no other impurities are presented in the XRD patterns. The octahedral $LiMn_{1.95}Mg_{0.05}O_4$ particles show narrow size distribution with regular morphology. When used as cathode material, the obtained $LiMn_{1.95}Mg_{0.05}O_4$ octahedra shows excellent electrochemical properties. This material can exhibit high capacity retention of 96.8% with 100th discharge capacity of 111.6 mAh g^{-1} at 1.0 C. Moreover, the rate performance and high-temperature cycling stability of $LiMn_2O_4$ are effectively improved by the co-modification strategy based on Mg-doping and octahedral morphology. These results are mostly given to the fact that the addition of magnesium ions can suppress the Jahn–Teller effect and the octahedral morphology contributes to the Mn dissolution, which can improve the structural stability of $LiMn_2O_4$.

Keywords: $LiMn_2O_4$; Mg-doping; octahedral morphology; synergistic effect; electrochemical properties

1. Introduction

With the increasingly serious environmental pollution, new energy and environmental technology have caught more and more extensive attention. Under this circumstance, the research and development of lithium-ion batteries are receiving more and more attention at home and abroad since their first commercial application in 1991 [1–3]. As an important cathode material, $LiMn_2O_4$ possesses a rather high cost advantage because of the abundant manganese resource and this material can be obtained by many preparation technologies [4–8]. Moreover, this material does not involve the use of toxic metal elements. All these advantages can promote large-scale applications of $LiMn_2O_4$. It must be noted, however, that the cycling stability and high temperature performance cannot meet the requirement of long endurance mileage [9–12].

According to the existing literature, the electrochemical performance of $LiMn_2O_4$ can be severely affected by the Jahn–Teller distortion effect and Mn dissolution during the process of discharging and charging due to the fact that the Jahn–Teller distortion and Mn dissolution is closely related to the trivalent state (Mn^{3+}), which can seriously affect the discharging process and the discharged state [13–16]. In recent years, many optimization strategies (doping, coating, morphology control, etc.) have been developed to address these problems [11,15,17–21]. Among them, the doping strategy

usually choses other heterogeneous ions (Li^+, Mg^{2+}, Zn^{2+}, Al^{3+}, Cr^{3+}, Si^{4+}, etc.) to replace a small amount of manganese ions [2,9,22–25]. As a result, the Jahn–Teller distortion effect can be decreased, which enhances the structural stability of $LiMn_2O_4$. Among these heterogeneous ions, magnesium has a wide distribution in nature and can work as an additive in electrolyte as well as an additive in cathode slurry [26,27]. More importantly, the addition of magnesium ions in $LiMn_2O_4$ can play a positive role in improving the electrochemical properties. Huang et al. [23] have prepared Mg-doped $LiMn_2O_4$ samples and investigated the effect of introducing magnesium ions on the structure, morphology, and cycling properties. The introduction of magnesium ions can strengthen the structural stability of $LiMn_2O_4$ by reducing the cell volume, and the reduction of trivalent manganese ions further strengthens the crystal structure of $LiMn_2O_4$ by suppressing the Jahn–Teller effect. The obtained Mg-doped $LiMn_2O_4$ sample can show higher capacity retention. Many other research works have confirmed the positive effect of introducing magnesium ions on optimizing the cycling properties of $LiMn_2O_4$ [28]. Furthermore, it has been reported that the high-performance $LiMn_2O_4$ can be prepared by solid-state method using Mn_3O_4 with octahedral morphology [29]. Zhao et al. [30] successfully prepared the octahedral $LiMn_2O_4$ particles by using Mn_3O_4 octahedra as manganese source. Since the octahedral morphology can suppress the dissolution of Mn to steady crystal structure, the obtained $LiMn_2O_4$ octahedra shows excellent electrochemical properties. Based on the above analysis, it is worth considering that the simultaneous use of the Mg-doping and octahedral morphology may greatly enhance the electrochemical properties of $LiMn_2O_4$.

Herein, the Mg-doped $LiMn_2O_4$ octahedra were prepared by high temperature solid-phase method with magnesium nitrate and Mn_3O_4 octahedra as doping agent and manganese source. The electrochemical properties of the octahedral $LiMn_{1.95}Mg_{0.05}O_4$ sample as cathode material were investigated in detail. It could be found that the electrochemical properties of $LiMn_2O_4$ were greatly enhanced by jointly using the Mg-doping and octahedral morphology. This work indicates that the co-modification strategy based on Mg-doping and octahedral morphology has vital significance to promote the practical application of $LiMn_2O_4$.

2. Materials and Methods

The octahedral $LiMn_{1.95}Mg_{0.05}O_4$ (LMMOO) particles were prepared by high temperature solid-phase method with magnesium nitrate and Mn_3O_4 octahedra as doping agent and manganese source. The octahedral Mn_3O_4 particles were firstly prepared via a hypothermal approach according to the existing literature [30]. Subsequently, in a typical synthesis process, stoichiometric $LiOH{\cdot}H_2O$, Mn_3O_4 octahedra, and $Mg(NO_3)_2{\cdot}6H_2O$ were ground to obtain the slurry mixture with the help of absolute ethanol. Then, the homogeneous mixture was dried in a drying oven and sintered at 700 °C for 10 h in air. In order to allow the comparison, the undoped $LiMn_2O_4$ (LMO) and $LiMn_{1.95}Mg_{0.05}O_4$ (LMMO) particles were prepared by using electrolytic MnO_2 as manganese precursor.

The structure and morphology usually have an important impact on the electrochemical properties of cathode material. The obtained $LiMn_2O_4$ and $LiMn_{1.95}Mg_{0.05}O_4$ samples were characterized by using XRD and SEM techniques. The effects of Mg-doping and octahedral morphology on the cycling stability of $LiMn_2O_4$ were studied by fabricating the coin cells with the obtained spinels as cathode materials. The positive electrode was constituted from 85% synthesized product as cathode material, 10% acetylene black as conductive agent, and 5% polyvinylidene fluoride dissolved in N-methyl-2-pyrrolidone as binder. The metallic lithium foil was used as counter electrode, the polypropylene microporous membrane was used as diaphragm, and the 1 M lithium hexafluorophosphate ($LiPF_6$) solution in a mixture of the ethylene carbonate (EC) and diethyl carbonate (DEC) at a volume ratio of 1:1 was used as the electrolyte. All the electrochemical tests were carried out on LANHE CT2001A system (LANHE, Wuhan, China) and CHI660E electrochemical workstation (CH Instruments, Shanghai, China).

3. Results and Discussion

In order to confirm the structures of the obtained samples, the $LiMn_2O_4$, $LiMn_{1.95}Mg_{0.05}O_4$, and octahedral $LiMn_{1.95}Mg_{0.05}O_4$ samples were characterized. It can be seen from Figure 1 that the diffraction peaks of the undoped $LiMn_2O_4$ are in good agreement with the standard diffraction peaks of $LiMn_2O_4$ (JCPDS No. 35-0782). No other diffraction peaks of manganese oxide and magnesium oxide can be observed, suggesting the complete transformation of electrolytic manganese dioxide to $LiMn_2O_4$ [31]. After introducing a small amount of magnesium ions, the obtained $LiMn_{1.95}Mg_{0.05}O_4$ sample was still present in the spinel cubic structure of $LiMn_2O_4$, which indicates that the addition of magnesium ions did not change the crystal structure [32,33]. For the $LiMn_{1.95}Mg_{0.05}O_4$ sample obtained from Mn_3O_4 octahedra, the characteristic diffraction peaks were indexed to the spinel $LiMn_2O_4$. Moreover, the corresponding peak intensities are stronger than that of the $LiMn_2O_4$ and $LiMn_{1.95}Mg_{0.05}O_4$ samples prepared from electrolytic manganese dioxide, suggesting the good crystalline quality of the octahedral $LiMn_{1.95}Mg_{0.05}O_4$ sample [9,34]. Table 1 lists the related crystal parameters of these three samples. The addition of magnesium ions leads to the reduction of the lattice parameter and shrinking of unit cell volume, suggesting the more stable structural stability of the $LiMn_{1.95}Mg_{0.05}O_4$ samples.

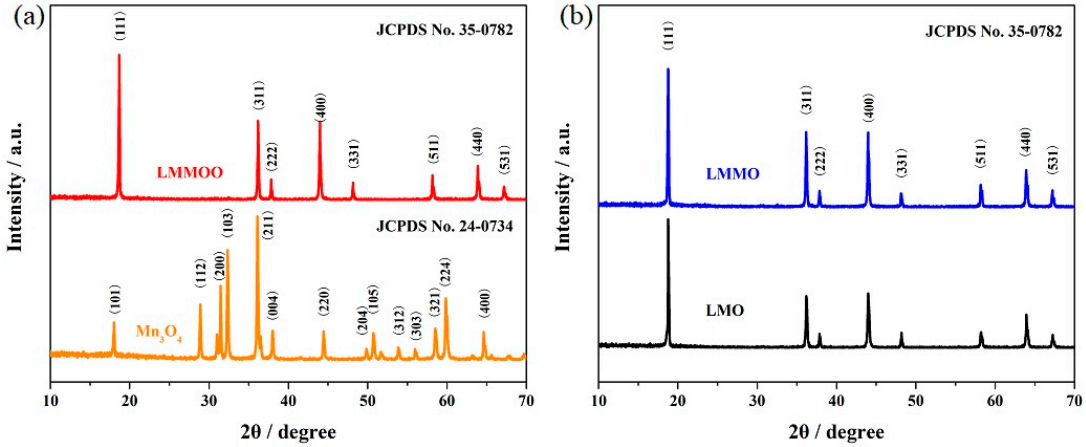

Figure 1. XRD patterns of (**a**) Mn_3O_4 and octahedral $LiMn_{1.95}Mg_{0.05}O_4$, and (**b**) $LiMn_2O_4$ and $LiMn_{1.95}Mg_{0.05}O_4$ samples.

Table 1. Crystal parameters of the $LiMn_2O_4$ and $LiMn_{1.95}Mg_{0.05}O_4$ samples.

Sample	Space	a (nm)	V (nm^3)
LMO	Fd-3m	0.82392	0.55931
LMMO	Fd-3m	0.82287	0.55718
LMMOO	Fd-3m	0.82253	0.55649

Figure 2 shows the SEM images of the octahedral Mn_3O_4, $LiMn_2O_4$, and Mg-doped $LiMn_2O_4$ samples. As shown in Figure 2a, the Mn_3O_4 particles prepared by hydrothermal approach present rather good octahedral morphology. For the octahedral $LiMn_{1.95}Mg_{0.05}O_4$ sample shown in Figure 2b,c, it can be seen that it presents a narrow size distribution with regular morphology, which indicates that the $LiMn_{1.95}Mg_{0.05}O_4$ sample inherits the special morphology of Mn_3O_4 octahedra [30]. Moreover, the particle size belongs to the submicron scale, which agrees with the particle size of Mn_3O_4. By contrast, the particle morphology of the undoped $LiMn_2O_4$ particles (Figure 2d) is irregular with micron grade particle size. Especially, the obvious agglomerated particle can be observed in the undoped $LiMn_2O_4$ particles. These unsatisfactory characteristics usually have a greater negative impact on the electrochemical properties of the cathode material [35,36]. For the $LiMn_{1.95}Mg_{0.05}O_4$ sample (Figure 2e), it shows relatively good size distribution, which is closely related to the addition

of a certain amount of magnesium ions, which agrees with the research result [23,33]. These results suggest that the combination of Mg-doping and octahedral morphology can be useful in optimizing the morphology and size distribution of $LiMn_2O_4$ particles.

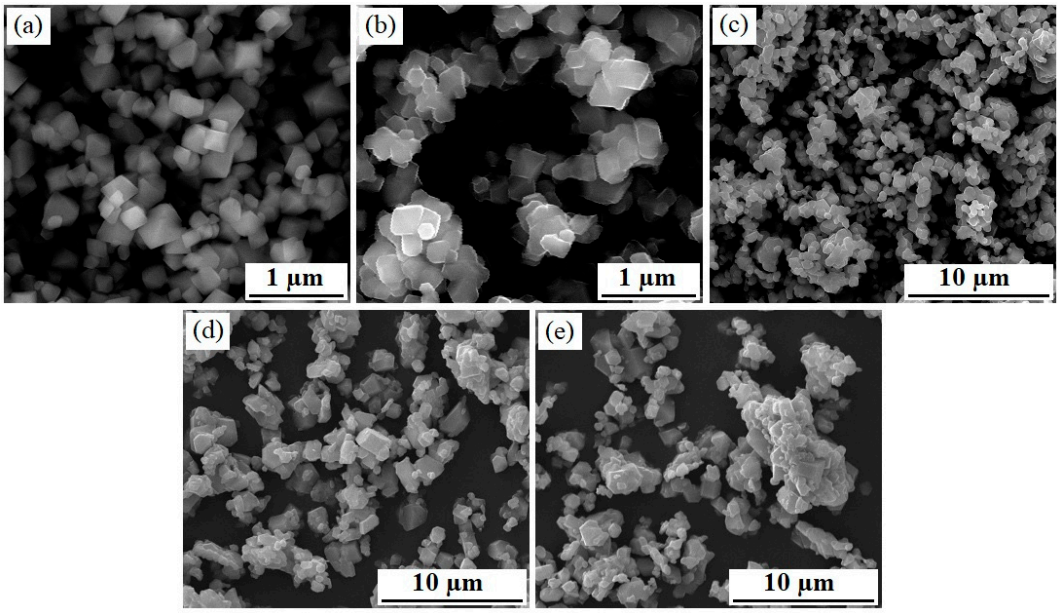

Figure 2. SEM images of (**a**) Mn_3O_4 octahedra, (**b**,**c**) $LiMn_{1.95}Mg_{0.05}O_4$ octahedra, (**d**) $LiMn_2O_4$, and (**e**) $LiMn_{1.95}Mg_{0.05}O_4$.

To investigate the influence of jointly using the Mg-doping and octahedral morphology on the electrochemical performance, the $LiMn_2O_4$, $LiMn_{1.95}Mg_{0.05}O_4$, and octahedral $LiMn_{1.95}Mg_{0.05}O_4$ samples were tested at a cycling rate of 1.0 C, the corresponding initial charge–discharge curves are shown in Figure 3. It can be seen that the undoped $LiMn_2O_4$ sample exhibits characteristic discharge curves of $LiMn_2O_4$ with two voltage plateaus. According to the research result [37,38], these two voltage plateaus correspond to the intercalation/de-intercalation processes of lithium ions, which correspond to the two-phase equilibrium of λ-MnO_2/$Li_{0.5}Mn_2O_4$ and single-phase equilibrium of $Li_{0.5}Mn_2O_4$/$LiMn_2O_4$, respectively. For the $LiMn_{1.95}Mg_{0.05}O_4$ and octahedral $LiMn_{1.95}Mg_{0.05}O_4$ samples, the initial charge–discharge curves show similar platform characteristics, and the potential interval of the Mg-doped spinels is less than that of the undoped spinel, suggesting the higher reaction kinetics of the Mg-doped spinels [39]. It is important to note, however, that the discharge voltage plateaus of the $LiMn_{1.95}Mg_{0.05}O_4$ samples are slightly higher than that of the undoped $LiMn_2O_4$ sample, which may be related to the optimization of the Li^+ intercalation/deintercalation behaviors due to the addition of other cations in the spinel structure [10,33,39,40].

The cycling performance is a very important index sign for the practical application of $LiMn_2O_4$. Figure 4 shows the cycling stability of the $LiMn_2O_4$, $LiMn_{1.95}Mg_{0.05}O_4$, and octahedral $LiMn_{1.95}Mg_{0.05}O_4$ samples at 1.0 C. For the undoped $LiMn_2O_4$ sample, it exhibits an initial capacity of 116.6 mAh g^{-1} with unsatisfactory cycling stability. After 100 cycles, the discharge capacity presents much decrease with the 100th capacity of 83.5 mAh g^{-1}. Such poor performance is mainly attributed to the wide size distribution and large agglomerated particle [35]. When adding some magnesium ions, the $LiMn_{1.95}Mg_{0.05}O_4$ sample shows higher capacity retention than that of undoped $LiMn_2O_4$ sample. Although the addition of magnesium ions decreases the initial discharge capacity, the capacity retention of the $LiMn_{1.95}Mg_{0.05}O_4$ sample is enhanced greatly. After 100 cycles, the discharge capacity can maintain 100.1 mAh g^{-1} with high retention of 89.5%. The improvement in cycling stability is attributed to the fact that the introduction of magnesium ions can strengthen the structural stability of $LiMn_2O_4$ by inhibiting the Jahn–Teller effect and reducing the cell volume [23,33]. It is important to note that the octahedral $LiMn_{1.95}Mg_{0.05}O_4$ sample can show more excellent cycling performance.

Compared with the undoped $LiMn_2O_4$ and $LiMn_{1.95}Mg_{0.05}O_4$ samples, the capacity retention of the octahedral $LiMn_{1.95}Mg_{0.05}O_4$ sample can reach up to 96.8% after 100 cycles with the 100th capacity of 111.6 mAh g^{-1}. Such excellent cycling stability mainly benefits from the synergistic effect of the Mg-doping and octahedral morphology. The Mg-doping can suppress the Jahn–Teller effect and the octahedral morphology can contribute to inhibit the Mn dissolution, which can improve the structural stability of $LiMn_2O_4$ [29,36].

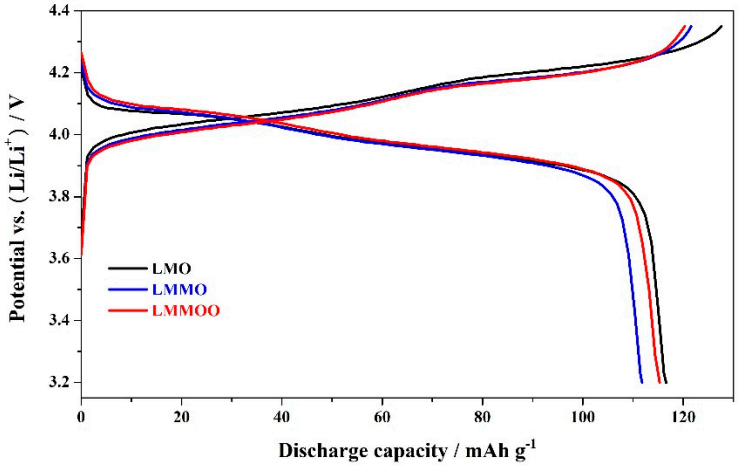

Figure 3. Initial charge–discharge curves of the $LiMn_2O_4$, $LiMn_{1.95}Mg_{0.05}O_4$, and octahedral $LiMn_{1.95}Mg_{0.05}O_4$ samples at 1.0 C.

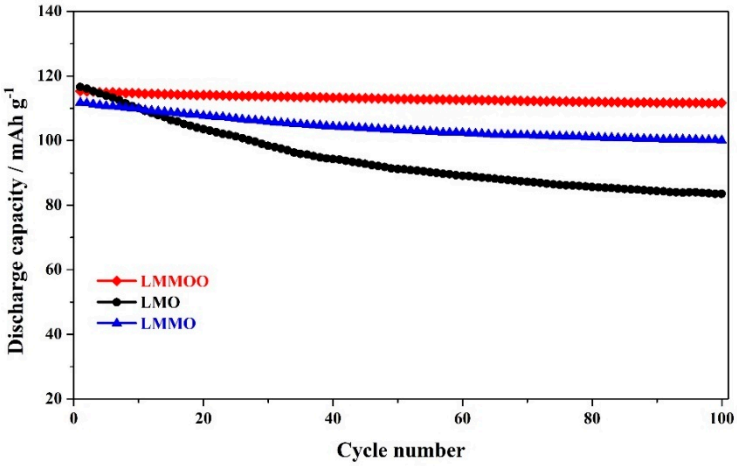

Figure 4. Cycling stability of the $LiMn_2O_4$, $LiMn_{1.95}Mg_{0.05}O_4$, and octahedral $LiMn_{1.95}Mg_{0.05}O_4$ samples at 1.0 C.

To investigate the effect of jointly using the Mg-doping and octahedral morphology on the rate capability, the $LiMn_2O_4$, $LiMn_{1.95}Mg_{0.05}O_4$, and octahedral $LiMn_{1.95}Mg_{0.05}O_4$ samples were successively cycled at 0.5, 1.0, 2.0, and 5.0 C, respectively. Figure 5a presents the characteristic discharge curves of the octahedral $LiMn_{1.95}Mg_{0.05}O_4$ sample (the representative of these three samples) at different cycling rates. As shown here, the discharge capacity and voltage platform are significantly affected by the high cycling rate. When the cycling rate gradually increases, the boundary of the two voltage plateaus become smooth and fuzzy and the discharge capacity gradually decreases due to the increased polarization, which are in accordance with the existing literature [41–43]. Figure 5b shows the corresponding cycling performance of the $LiMn_2O_4$, $LiMn_{1.95}Mg_{0.05}O_4$, and octahedral $LiMn_{1.95}Mg_{0.05}O_4$ samples at varying cycling rates. The undoped $LiMn_2O_4$ sample exhibits a discharge capacity of 126.7 mAh g^{-1} at low cycling rate of 0.5 C. With the increase of the cycling rates, the discharge capacity is influenced greatly. As the cycling rate increases to 5.0 C, the undoped $LiMn_2O_4$ sample only

exhibits 55.0 mAh g^{-1} with rather low retention of 43.4%. By contrast, the Mg-doped $LiMn_2O_4$ samples present outstanding cycling stability at high cycling rate. Especially, the octahedral $LiMn_{1.95}Mg_{0.05}O_4$ sample can exhibit a higher capacity of 91.8 mAh g^{-1} at a high cycling rate of 5.0 C. To further explore the high-rate cycling stability, the octahedral $LiMn_{1.95}Mg_{0.05}O_4$ samples were cycled at 10 C. The corresponding characteristic discharge curves are shown in Figure 6a. It can be found that the characteristic voltage plateaus in the discharge curves become blurred to a large extent, which agrees with the research result [39,44,45]. Figure 6b presents the cycling performance of the octahedral $LiMn_{1.95}Mg_{0.05}O_4$ samples at 10 C. It can show satisfactory retention of 97.5% after 100 cycles with initial capacity of 72.1 mAh g^{-1}. The above results suggest that the co-modification strategy based on Mg-doping and octahedral morphology is an important means for effectively improving the rate capability of $LiMn_2O_4$.

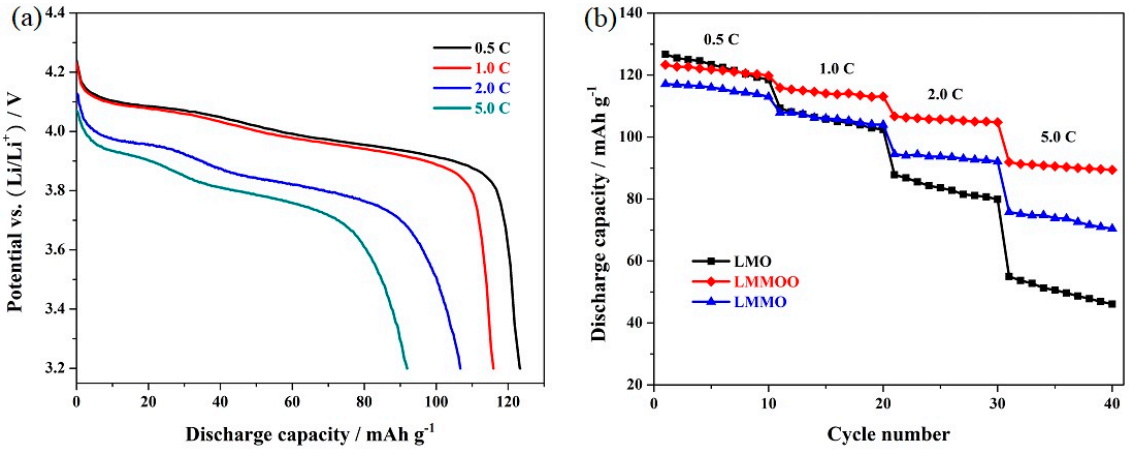

Figure 5. (**a**) Representative discharge curves of the octahedral $LiMn_{1.95}Mg_{0.05}O_4$ sample and (**b**) rate capability of the $LiMn_2O_4$, $LiMn_{1.95}Mg_{0.05}O_4$, and octahedral $LiMn_{1.95}Mg_{0.05}O_4$ samples.

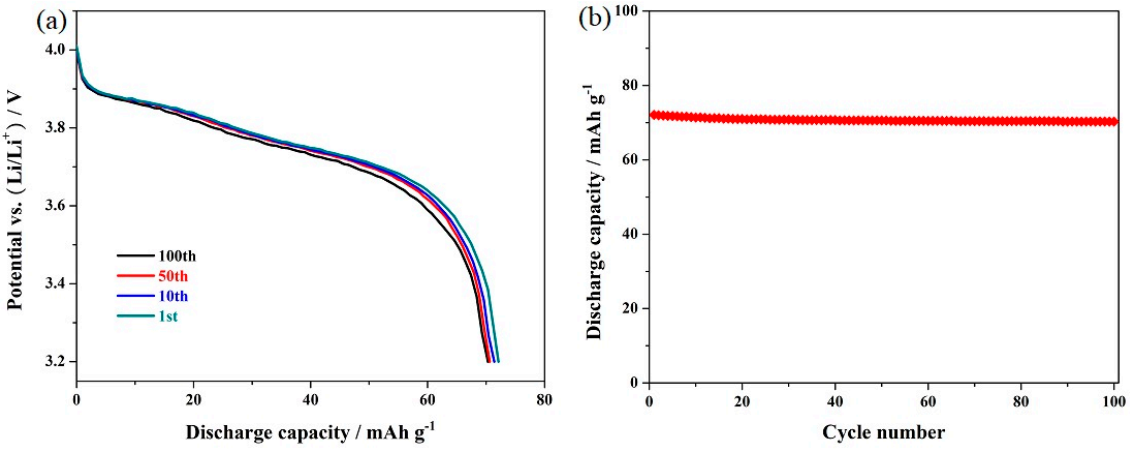

Figure 6. (**a**) Initial discharge curves and (**b**) cycling performance of the octahedral $LiMn_{1.95}Mg_{0.05}O_4$ sample at 10 C.

Figure 7a presents the high-temperature cycling stability of the $LiMn_2O_4$ and octahedral $LiMn_{1.95}Mg_{0.05}O_4$ samples at 1.0 C. It can be seen that the cycling stability of the undoped $LiMn_2O_4$ sample is much poorer than that of the octahedral Mg-doped $LiMn_2O_4$ sample. The initial discharge capacity of the undoped $LiMn_2O_4$ sample is comparable to the test results shown in Figure 4, but the capacity retention is rather poor. After 50 cycles, this sample only presents low capacity retention of 80.5%. It is important to note that the octahedral $LiMn_{1.95}Mg_{0.05}O_4$ can present excellent capacity retention of 92.5% with a satisfactory 50th discharge capacity of 106.6 mAh g^{-1}. Figure 7b shows the rate capability of the $LiMn_2O_4$ and octahedral $LiMn_{1.95}Mg_{0.05}O_4$ samples at 55 °C. As shown

here, the octahedral $LiMn_{1.95}Mg_{0.05}O_4$ sample shows more stable high-temperature cycling stability at different rates, especially the high cycling rate. When tested at 5.0 C, the octahedral $LiMn_{1.95}Mg_{0.05}O_4$ sample can maintain the discharge capacity of 95.6 mAh g^{-1}. Unfortunately, the undoped $LiMn_2O_4$ sample presents unsatisfactory rate capability, which further confirms the synergistic effect of the Mg-doping and octahedral morphology.

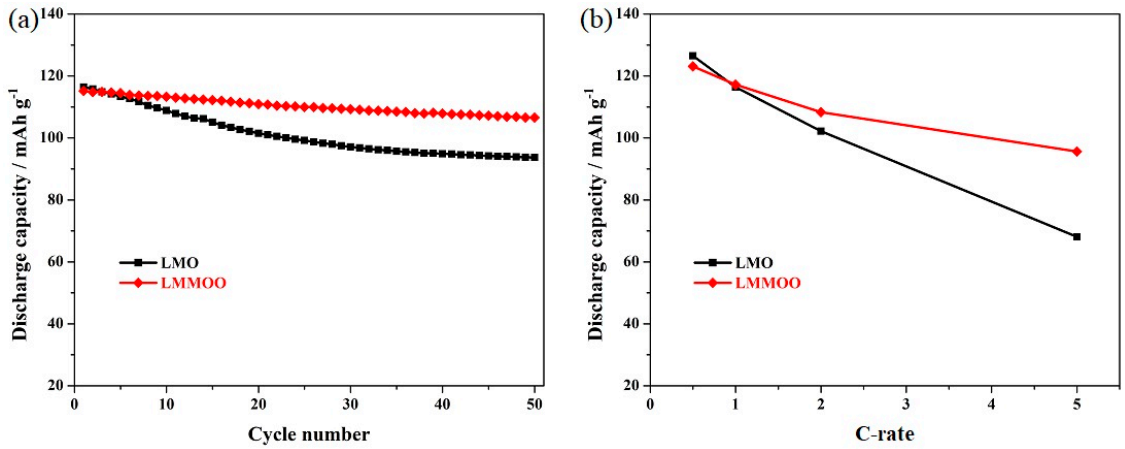

Figure 7. (**a**) Cycling stability of the $LiMn_2O_4$ and octahedral $LiMn_{1.95}Mg_{0.05}O_4$ samples at 1.0 C under high temperature (55 °C), and (**b**) representative discharge curves of the octahedral $LiMn_{1.95}Mg_{0.05}O_4$ sample.

Figure 8a presents the Nyquist plots of the $LiMn_2O_4$ and octahedral $LiMn_{1.95}Mg_{0.05}O_4$ samples, and Figure 8b shows the corresponding equivalent circuit model. According to the research result [9,10,23], the charge transfer resistance (R_2) in the high-frequency region has strong ties to the electrochemical properties. Therefore, we mainly studied the R_2 value to confirm the effect of both the Mg-doping and octahedral morphology on the electrochemical performance. As shown in Figure 8a, the combination of Mg-doping and octahedral morphology produces an important influence on the R_2 value. The addition of magnesium ions can suppress the Jahn–Teller distortion effect to improve the structural stability, and the octahedral morphology of $LiMn_2O_4$ octahedra suppresses the dissolution of Mn in electrolyte [30,36]. Moreover, the uniform particle size distribution also contributes to the diffusion efficiency of lithium ions [33,39,43]. As a result, the octahedral $LiMn_{1.95}Mg_{0.05}O_4$ sample presents lower initial charge-transfer resistance than that of the undoped spinel, which suggests excellent electrochemical properties.

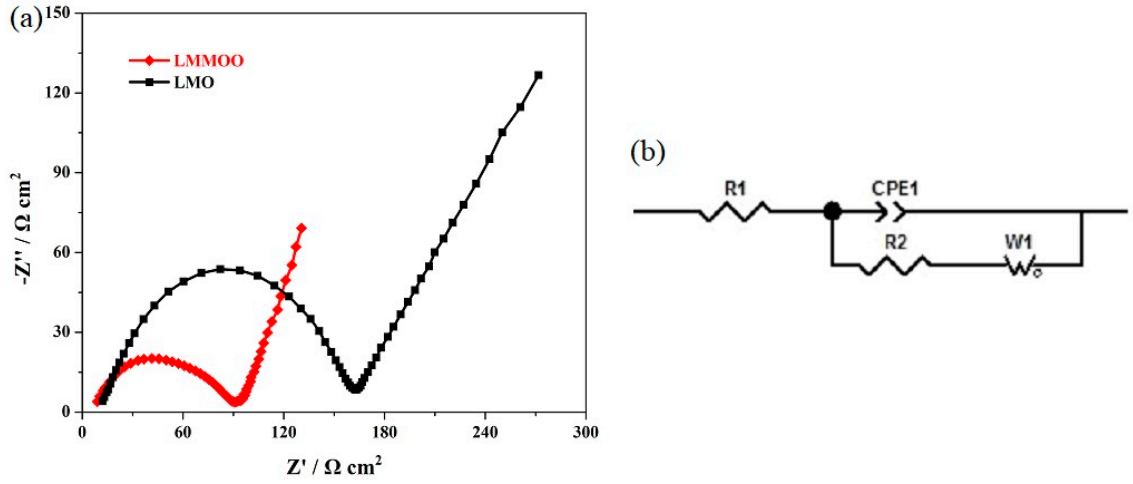

Figure 8. (**a**) Nyquist plots of the $LiMn_2O_4$ and octahedral $LiMn_{1.95}Mg_{0.05}O_4$ samples and (**b**) equivalent circuit model of EIS.

4. Conclusions

To summarize, the octahedral $LiMn_{1.95}Mg_{0.05}O_4$ sample was prepared by high temperature solid-phase method with magnesium nitrate and Mn_3O_4 octahedra as the doping agent and manganese source. XRD and SEM results indicate that the Mg-doping does not change the structure of $LiMn_2O_4$ and the octahedral morphology of manganese source is inherited well in the obtained $LiMn_{1.95}Mg_{0.05}O_4$ sample. The synergistic effect of both the Mg-doping and octahedral morphology on the electrochemical performance were confirmed. The octahedral $LiMn_{1.95}Mg_{0.05}O_4$ sample can show more excellent electrochemical properties compared to the undoped $LiMn_2O_4$ and $LiMn_{1.95}Mg_{0.05}O_4$ particles. When cycled at 1.0 C, the capacity retention of the $LiMn_{1.95}Mg_{0.05}O_4$ sample can reach up to 96.8% after 100 cycles with the initial capacity of 115.3 mAh g^{-1}. Not only that, the combination of Mg-doping and octahedral morphology also significantly enhances the rate capability and high-temperature performance. This work is meaningful to promote the large-scale commercial application of $LiMn_2O_4$.

Author Contributions: H.Z. and Y.L. conceived and designed the experiments; H.Z. and Y.N. performed the experiments; all authors analyzed the data; H.Z. wrote the paper; all authors discussed the results and commented on the paper.

Funding: This research was funded by the Key Research Project of Education Department of Henan Province (No. 19A150023, No. 19A430014), Research Project of Science and Technology of Henan Province (No. 192102210301, No. 192102210215), High-Level Talents Introduction Project of Henan Institute of Science and Technology (No. 203010617011), and Program for Innovative Research Team (in Science and Technology) in University of Henan Province (No. 20IRTSTHN016).

Conflicts of Interest: The authors declare no conflict of interest.

References

1. Li, M.; Lu, J.; Chen, Z.; Amine, K. 30 years of lithium-ion batteries. *Adv. Mater.* **2018**, *30*, 1800561. [CrossRef] [PubMed]
2. Zhao, H.; Li, D.; Wang, Y.; Li, F.; Wang, G.; Wu, T.; Wang, Z.; Li, Y.; Su, J. Sol-gel synthesis of silicon-doped lithium manganese oxide with enhanced reversible capacity and cycling stability. *Materials* **2018**, *11*, 1455. [CrossRef] [PubMed]
3. Normakhmedov, O.O.; Brylev, O.A.; Petukhov, D.I.; Kurilenko, K.A.; Kulova, T.L.; Tuseeva, E.K.; Skundin, A.M. Cryochemically processed $Li_{1+y}Mn_{1.95}Ni_{0.025}Co_{0.025}O_4$ (y = 0, 0.1) cathode materials for Li-ion batteries. *Materials* **2018**, *11*, 1162. [CrossRef] [PubMed]
4. Huang, W.; Wang, G.; Luo, C.; Xu, Y.; Xu, Y.; Eckstein, B.J.; Chen, Y.; Wang, B.; Huang, J.; Kang, Y.; et al. Controllable growth of $LiMn_2O_4$ by carbohydrate-assisted combustion synthesis for high performance Li-ion batteries. *Nano Energy* **2019**, *64*, 103936. [CrossRef]
5. Lu, J.; Zhou, C.; Liu, Z.; Lee, K.S.; Lu, L. $LiMn_2O_4$ cathode materials with large porous structure and radial interior channels for lithium ion batteries. *Electrochim. Acta* **2016**, *212*, 553–560. [CrossRef]
6. Hou, Y.; Chang, K.; Tang, H.; Li, B.; Hou, Y.; Chang, Z. Drastic enhancement in the rate and cyclic behavior of $LiMn_2O_4$ electrodes at elevated temperatures by phosphorus doping. *Electrochim. Acta* **2019**, *319*, 587–595. [CrossRef]
7. Han, C.G.; Zhu, C.; Saito, G.; Akiyama, T. Improved electrochemical performance of $LiMn_2O_4$ surface-modified by a Mn^{4+}-rich phase for rechargeable lithium-ion batteries. *Electrochim. Acta* **2016**, *209*, 225–234. [CrossRef]
8. Pyun, M.H.; Park, Y.J. Graphene/$LiMn_2O_4$ nanocomposites for enhanced lithium ion batteries with high rate capability. *J. Alloys Compd.* **2015**, *643*, 90–94. [CrossRef]
9. Zhao, H.; Gao, X.; Li, Y.; Ran, Q.; Fu, C.; Feng, Y.; Liu, J.; Liu, X.; Su, J. Synergistic effects of zinc-doping and nano-rod morphology on enhancing the electrochemical properties of spinel Li-Mn-O material. *Ceram. Int.* **2019**, *45*, 17591–17597. [CrossRef]
10. Zhao, H.; Li, F.; Bai, X.; Wu, T.; Wang, Z.; Li, Y.; Su, J. Enhanced cycling stability of $LiCu_xMn_{1.95-x}Si_{0.05}O_4$ cathode material obtained by solid-state method. *Materials* **2018**, *11*, 1302. [CrossRef]

11. Zhang, C.; Su, J.; Wang, T.; Yuan, K.; Chen, C.; Liu, S.; Huang, T.; Wu, J.; Lu, H.; Yu, A. Significant improvement on electrochemical performance of $LiMn_2O_4$ at elevated temperature by atomic layer deposition of TiO_2 nanocoating. *ACS Sustain. Chem. Eng.* **2018**, *6*, 7890–7901. [CrossRef]
12. Wang, H.Q.; Lai, F.Y.; Li, Y.; Zhang, X.H.; Huang, Y.G.; Hu, S.J.; Li, Q.Y. Excellent stability of spinel $LiMn_2O_4$-based cathode materials for lithium-ion batteries. *Electrochim. Acta* **2015**, *177*, 290–297. [CrossRef]
13. Rodríguez, R.A.; Pérez–Cappe, E.L.; Laffita, Y.M.; Ardanza, A.C.; Salazar, J.S.; Santos, M.Á.; Aguilar Frutis, M.A.; Mohalem, N.D.S.; Alves, O.L. Structural defects in $LiMn_2O_4$ induced by gamma radiation and its influence on the Jahn-Teller effect. *Solid State Ion.* **2018**, *324*, 77–86. [CrossRef]
14. Qiao, Y.; Zhou, Z.; Chen, Z.; Du, S.; Cheng, Q.; Zhai, H.; Fritz, N.J.; Du, Q.; Yang, Y. Visualizing ion diffusion in battery systems by fluorescence microscopy: A case study on the dissolution of $LiMn_2O_4$. *Nano Energy* **2018**, *45*, 68–74. [CrossRef]
15. Kasnatscheew, J.; Wagner, R.; Winter, M.; Cekic–Laskovic, I. *Interfaces and Materials in Lithium Ion Batteries: Challenges for Theoretical Electrochemistry*; Springer: Cham, Switzerland, 2018; Volume 376, p. 16.
16. Tao, S.; Zhao, H.; Wu, C.; Xie, H.; Cui, P.; Xiang, T.; Chen, S.; Zhang, L.; Fang, Y.; Wang, Z.; et al. Enhanced electrochemical performance of MoO_3-coated $LiMn_2O_4$ cathode for rechargeable lithium-ion batteries. *Mater. Chem. Phys.* **2017**, *199*, 203–208. [CrossRef]
17. Mao, Y.; Xiao, S.; Liu, J. Nanoparticle-assembled $LiMn_2O_4$ hollow microspheres as high-performance lithium-ion battery cathode. *Mater. Res. Bull.* **2017**, *96*, 437–442. [CrossRef]
18. Zhao, H.; Liu, S.; Wang, Z.; Cai, Y.; Tan, M.; Liu, X. Enhanced elevated-temperature performance of $LiAl_xSi_{0.05}Mg_{0.05}Mn_{1.90-x}O_4$ ($0 \le x \le 0.08$) cathode materials for high-performance lithium-ion batteries. *Electrochim. Acta* **2016**, *199*, 18–26. [CrossRef]
19. Tron, A.; Park, Y.D.; Mun, J. AlF_3-coated $LiMn_2O_4$ as cathode material for aqueous rechargeable lithium battery with improved cycling stability. *J. Power Sources* **2016**, *325*, 360–364. [CrossRef]
20. Michalska, M.; Ziółkowska, D.A.; Jasiński, J.B.; Lee, P.H.; Ławniczak, P.; Andrzejewski, B.; Ostrowski, A.; Bednarski, W.; Wu, S.H.; Lin, J.Y. Improved electrochemical performance of $LiMn_2O_4$ cathode material by Ce doping. *Electrochim. Acta* **2018**, *276*, 37–46. [CrossRef]
21. Wu, Y.; Cao, C.; Zhang, J.; Wang, L.; Ma, X.; Xu, X. Hierarchical $LiMn_2O_4$ hollow cubes with exposed {111} planes as high-power cathodes for lithium–ion batteries. *ACS Appl. Mater. Interfaces* **2016**, *8*, 19567–19572. [CrossRef]
22. Sheth, J.; Karan, N.K.; Abraham, D.P.; Nguyen, C.C.; Lucht, B.L.; Sheldon, B.W.; Guduru, P.R. In situ stress evolution in $Li_{1+x}Mn_2O_4$ thin films during electrochemical cycling in Li-ion cells. *J. Electrochem. Soc.* **2016**, *163*, 2524–2530. [CrossRef]
23. Huang, J.; Yang, F.; Guo, Y.; Peng, C.; Bai, H.; Peng, J.; Guo, J. $LiMg_xMn_{2-x}O_4$ ($x \le 0.10$) cathode materials with high rate performance prepared by molten-salt combustion at low temperature. *Ceram. Int.* **2015**, *41*, 9662–9667. [CrossRef]
24. Peng, C.; Huang, J.; Guo, Y.; Li, Q.; Bai, H.; He, Y.; Su, C.; Guo, J. Electrochemical performance of spinel $LiAl_xMn_{2-x}O_4$ prepared rapidly by glucose-assisted solid-state combustion synthesis. *Vacuum* **2015**, *120*, 121–126. [CrossRef]
25. Song, H.; Zhao, Y.; Niu, Y.; Wu, Z.; Hou, H. Applications of $LiCr_xMn_{2-x}O_4$ cathode material with high capacity and high rate in high-temperature battery. *Solid State Ion.* **2018**, *325*, 67–73. [CrossRef]
26. Wagner, R.; Streipert, B.; Kraft, V.; Reyes Jiménez, A.; Röser, S.; Kasnatscheew, J.; Gallus, D.R.; Börner, M.; Mayer, C.; Arlinghaus, H.F.; et al. Counterintuitive role of magnesium salts as effective electrolyte additives for high voltage lithium-ion batteries. *Adv. Mater. Interfaces* **2016**, *3*, 1600096. [CrossRef]
27. Wagner, R.; Kraft, V.; Streipert, B.; Kasnatscheew, J.; Gallus, D.R.; Amereller, M.; Korth, M.; Cekic–Laskovic, I.; Winter, M. Magnesium-based additives for the cathode slurry to enable high voltage application of lithium–ion batteries. *Electrochim. Acta* **2018**, *228*, 9–17. [CrossRef]
28. Guo, J.; Hu, L.; Su, C.; Wang, R.; Liu, X.; Peng, J.G. Effect of temperature on electrochemical performance of $LiMg_{0.06}Mn_{1.94}O_4$ prepared by a molten-salt combustion method. *Int. J. Electrochem. Sci.* **2016**, *11*, 4771–4778. [CrossRef]
29. Jin, G.; Qiao, H.; Xie, H.; Wang, H.; He, K.; Liu, P.; Chen, J.; Tang, Y.; Liu, S.; Huang, C. Synthesis of single-crystalline octahedral $LiMn_2O_4$ as high performance cathode for Li-ion battery. *Electrochim. Acta* **2014**, *150*, 1–7. [CrossRef]

30. Zhao, H.; Nie, Y.; Li, Y.; Wu, T.; Zhao, E.; Song, J.; Komarneni, S. Low-cost and eco-friendly synthesis of octahedral $LiMn_2O_4$ cathode material with excellent electrochemical performance. *Ceram. Int.* **2019**, *45*, 17183–17191. [CrossRef]
31. Zhao, H.; Li, F.; Liu, X.; Xiong, W.; Chen, B.; Shao, H.; Que, D.; Zhang, Z.; Wu, Y. A simple, low-cost and eco-friendly approach to synthesize single-crystalline $LiMn_2O_4$ nanorods with high electrochemical performance for lithium-ion batteries. *Electrochim. Acta* **2015**, *166*, 124–133. [CrossRef]
32. Li, G.; Yu, Y.; liu, J.; Feng, T.; Shao, M.; Su, C.; Guo, J. Study on electrochemical performance of $LiMg_{0.06}Mn_{1.94}O_4$ synthesized by solid–state combustion method. *Int. J. Electrochem. Sci.* **2018**, *13*, 1495–1504. [CrossRef]
33. Xiang, M.; Su, C.W.; Feng, L.; Yuan, M.; Guo, J. Rapid synthesis of high-cycling performance $LiMg_xMn_{2-x}O_4$ ($x \leq 0.20$) cathode materials by a low-temperature solid-state combustion method. *Electrochim. Acta* **2014**, *125*, 524–529. [CrossRef]
34. Liu, S.; Zhao, H.; Tan, M.; Hu, Y.; Shu, X.; Zhang, M.; Chen, B.; Liu, X. Er-doped $LiNi_{0.5}Mn_{1.5}O_4$ cathode material with enhanced cycling stability for lithium–ion batteries. *Materials* **2017**, *10*, 859. [CrossRef]
35. Chand, P.; Bansal, V.; Sukriti; Singh, V. Investigations of spinel $LiZn_xMn_{2-x}O_4$ ($x \leq 0.03$) cathode materials for a lithium ion battery application. *Mater. Sci. Eng. B Adv.* **2018**, *238*, 93–99. [CrossRef]
36. Feng, T.; Xu, W.; Liu, X.; Shao, M.; Guo, J.; Su, C. Effect of calcination time on lithium ion diffusion coefficient of $LiMg_{0.04}Mn_{1.96}O_4$ prepared by a solid-state combustion method. *Int. J. Electrochem. Sci.* **2018**, *13*, 1027–1041. [CrossRef]
37. Xiong, L.; Xu, Y.; Zhang, C.; Zhang, Z.; Li, J. Electrochemical properties of tetravalent Ti-doped spinel $LiMn_2O_4$. *J. Solid State Electr.* **2010**, *15*, 1263–1269. [CrossRef]
38. Zhang, H.; Xu, Y.; Liu, D.; Zhang, X.; Zhao, C. Structure and performance of dual-doped $LiMn_2O_4$ cathode materials prepared via microwave synthesis method. *Electrochim. Acta* **2014**, *125*, 225–231. [CrossRef]
39. Wen, W.; Ju, B.; Wang, X.; Wu, C.; Shu, H.; Yang, X. Effects of magnesium and fluorine co-doping on the structural and electrochemical performance of the spinel $LiMn_2O_4$ cathode materials. *Electrochim. Acta* **2014**, *147*, 271–278. [CrossRef]
40. Liu, H.; Tian, R.; Jiang, Y.; Tan, X.; Chen, J.; Zhang, L.; Guo, Y.; Wang, H.S.; Chu, W. On the drastically improved performance of Fe-doped $LiMn_2O_4$ nanoparticles prepared by a facile solution-gelation route. *Electrochim. Acta* **2015**, *180*, 138–146. [CrossRef]
41. Shang, Y.; Lin, X.; Lu, X.; Huang, T.; Yu, A. Nano-TiO_2 coated $LiMn_2O_4$ as cathode materials for lithium–ion batteries at elevated temperatures. *Electrochim. Acta* **2015**, *156*, 121–126. [CrossRef]
42. Liu, J.; Li, G.; Yu, Y.; Bai, H.; Shao, M.; Guo, J.; Su, C.; Liu, X.; Bai, W. Synthesis and electrochemical performance evaluations of polyhedra spinel $LiAl_xMn_{2-x}O_4$ ($x \leq 0.20$) cathode materials prepared by a solution combustion technique. *J. Alloys Compd.* **2017**, *728*, 1315–1328. [CrossRef]
43. Xiong, L.; Xu, Y.; Tao, T.; Goodenough, J.B. Synthesis and electrochemical characterization of multi-cations doped spinel $LiMn_2O_4$ used for lithium ion batteries. *J. Power Sources* **2012**, *199*, 214–219. [CrossRef]
44. Lai, F.; Zhang, X.; Wang, H.; Hu, S.; Wu, X.; Wu, Q.; Huang, Y.; He, Z.; Li, Q. Three-dimension hierarchical Al_2O_3 nanosheets wrapped $LiMn_2O_4$ with enhanced cycling stability as cathode material for lithium ion batteries. *ACS Appl. Mater. Interfaces* **2016**, *8*, 21656–21665. [CrossRef] [PubMed]
45. Kumar, N.; Rodriguez, J.R.; Pol, V.G.; Sen, A. Facile synthesis of 2D graphene oxide sheet enveloping ultrafine 1D $LiMn_2O_4$ as interconnected framework to enhance cathodic property for Li-ion battery. *Appl. Surf. Sci.* **2019**, *463*, 132–140. [CrossRef]